Selecting the tip electron orbital for scanning tunneling microscopy imaging with sub-ångström lateral resolution

2010 EPL 92 46003

(http://iopscience.iop.org/0295-5075/92/4/46003)

A Letters Journal Exploring the Frontiers of Physics

November 2010

EPL, **92** (2010) 46003
doi: 10.1209/0295-5075/92/46003

www.epljournal.org

Selecting the tip electron orbital for scanning tunneling microscopy imaging with sub-ångström lateral resolution

A. N. Chaika[1(a)], S. S. Nazin[1], V. N. Semenov[1], S. I. Bozhko[1,2], O. Lübben[2], S. A. Krasnikov[2], K. Radican[2] and I. V. Shvets[2]

[1] *Institute of Solid State Physics RAS - Chernogolovka, Moscow district 142432, Russia*
[2] *Centre for Research on Adaptive Nanostructures and Nanodevices (CRANN), School of Physics, Trinity College Dublin - Dublin 2, Ireland, EU*

received 17 August 2010; accepted in final form 27 October 2010
published online 6 December 2010

PACS 68.37.Ef – Scanning tunneling microscopy (including chemistry induced with STM)
PACS 73.40.Gk – Tunneling
PACS 73.20.At – Surface states, band structure, electron density of states

Abstract – We report on scanning tunneling microscopy (STM) studies performed with single crystalline W[001] tips on a graphite(0001) surface. Results of distance-dependent STM experiments with sub-ångström lateral resolution and density functional theory electronic structure calculations show how to controllably select one of the tip electron orbitals for high-resolution STM imaging. This is confirmed by experimental images reproducing the shape of the $5d_{xz,yz}$ and $5d_{x^2-y^2}$ tungsten atomic orbitals. The presented data demonstrate that the application of oriented single crystalline probes can provide further control of spatial resolution and expand the capabilities of STM.

In quantum mechanics, a single-electron state in an atom is described by a set of wave functions associated with a particular electron energy, orbital momentum, spin and momentum projections on the quantization axis. The spatial distribution of these wave functions (atomic orbitals) determines the probability for an electron with quantum numbers n, l, m_l, m_s to be detected in a particular volume of space. This theoretical formalism allows to explain the behavior of the electron systems on the atomic level. However, for a long time the electron orbitals could not be directly observed in experiments. This only became possible with invention of scanning probe microscopy (SPM) methods [1–3]. These use sharp tips to image [4] and manipulate [5] atomic structures, to identify the chemical nature of atomic species [6,7] and to reveal magnetic contrast [8] on surfaces.

The ultimate vertical resolution of scanning tunneling microscopy (STM) is determined by exponential dependence of the tunneling current between a sample and a tip [9]. The lateral resolution can be limited by the technical characteristics of a microscope. One of the first theoretical explanations of the atomic resolution was proposed by Tersoff and Hamann [10,11] who considered a spherically symmetric s-wave tip. The theory was further advanced by Chen [12–14] who showed that the tunneling matrix elements are proportional to the derivatives of the wave functions of electrons involved in the tunneling process. Therefore, a variety of electron states can contribute to experimental images and, consequently, the limit of lateral resolution is physically restricted by spatial distribution of the tip and surface wave functions. However, it took two decades after the invention of STM to measure the asymmetric charge distribution related to apex atomic orbitals in atomic force microscopy (AFM) [15,16] and STM [17–19] experiments. The observed subatomic features [15–19] still could not be unambiguously identified with single-electron orbitals. Recently, two legs of the MnNi tip d_{xz}-orbital ($l=2$, $m_l=1$) were resolved in STM experiments on a Cu(014)-O surface [20,21]. Essential distance dependence of the atomically resolved Cu(014)-O STM images [21,22], however, did not allow to reveal the conditions where this tip orbital channels most of the tunneling current. The observed distance dependence, leading to chemical selective imaging either copper or oxygen atomic rows of the Cu(014)-O surface [7,21,22], was attributed to change of relative contribution of different electron orbitals of the surface atoms. However, the distance-dependent contribution of different d-orbitals could be proved experimentally only by direct experiments demonstrating

(a) E-mail: chaika@issp.ac.ru

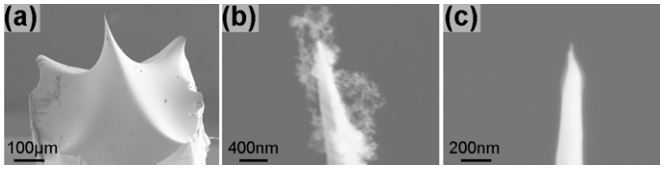

Fig. 1: (a)–(c) SEM images of electrochemically etched W[001] tips. Images in panels (a), (b) and (c) were taken from two different tips. The UHV tip treatment [23] is used to remove contaminants seen in panels (b), (c).

subatomic features of different symmetry at different gap spacings. For example, such experiments can be done using a combination of d electron tip states and s or p_z surface electron states.

In this work, we use the reciprocity principle of STM, and probe different d-orbitals of the W[001] tip atom by localized carbon orbitals of the highly oriented pyrolytic graphite (HOPG) surface atoms at different bias voltages and tip-sample separations. Using distance-dependent STM measurements with sub-ångström lateral resolution and density functional theory (DFT) calculations we demonstrate the possibility of selecting a particular tip electron orbital for high-resolution imaging. This is confirmed by reproducing the shapes of the W $5d_{xz,yz}$ and $5d_{x^2-y^2}$ atomic orbitals.

The experiments were carried out in an ultra-high vacuum (UHV, $p < 1 \times 10^{-10}$ mbar) chamber equipped with a room temperature STM (GPI-300). STM images were measured in the constant current mode. Tungsten tips were fabricated from [001]-oriented $0.5 \times 0.5 \times 10\,\mathrm{mm}^3$ single crystalline bars using electrochemical etching. Figure 1 shows typical scanning electron microscopy (SEM) images of chemically etched W[001] tips. Before the experiments, the tips were cleaned from contaminants and sharpened in the UHV chamber by electron beam heating and Ar^+ ion bombardment [23]. Only clean W[001] tips allowing to resolve a honeycomb surface structure (fig. 2(a)) directly after tip approach were used for all experiments. All other tip treatments (*e.g.*, continuous scanning or voltage pulses) which could lead to a mass transport from the sample to the tip were excluded. The distance dependence of the STM images was measured by varying the gap resistance with fixed bias voltages applied to the sample. Only sequences without tip changes were analyzed.

Figure 2(a) shows the atomic structure of graphite. Carbon atoms within each layer are strongly bonded via sp^2 bonds and form in-plane honeycomb patterns while the neighboring layers are weakly bonded via van der Waals forces. The honeycombs in the adjacent layers are shifted in the (x-y)-plane so that only three of six carbon atoms in each hexagon (namely, α atoms) lie directly above the atoms of the underlying layer, while the three others are located above the hollow sites (β atoms). Because of their non-equivalence, α and β atoms demonstrate different relaxations interacting with a SPM tip [24]. As a result, for most tunneling

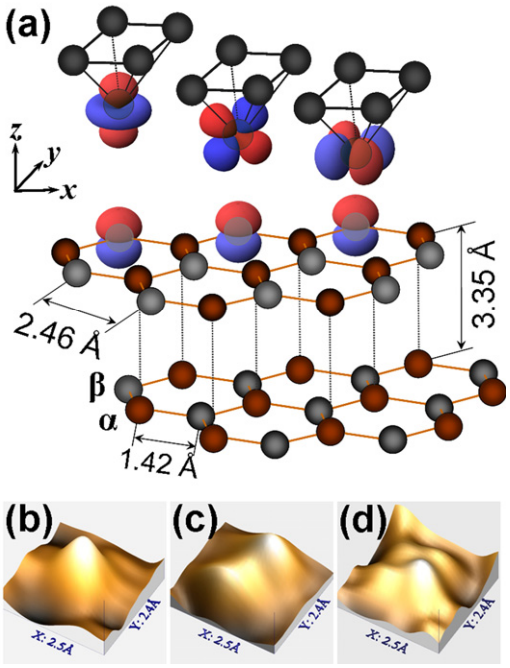

Fig. 2: (Color online) (a) Schematic view of a W[001] tip with the $d_{3z^2-r^2}$ (left), $d_{xz,yz}$ (center) or $d_{x^2-y^2}$ (right) orbital at the apex above the graphite surface. (b)–(d) Pseudo 3D images of the atomic features measured with W[001] tips at different tunneling parameters as indicated in fig. 6. The images are explained by overwhelming contribution of $d_{3z^2-r^2}$ (b), $d_{xz,yz}$ (c) or $d_{x^2-y^2}$ (d) electron states of the tip atom. $2.5 \times 2.4\,\mathrm{Å}^2$ STM images were plotted with the WSxM software [25].

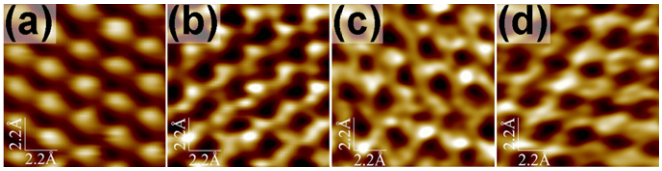

Fig. 3: (Color online) (a)–(d) $11 \times 11\,\mathrm{Å}^2$ STM images of HOPG(0001) measured with polycrystalline W tips. The images demonstrate a typical hexagonal pattern (a) and subatomic features with two- (b), three- (c) and four-fold (d) symmetry. The tunneling parameters are $U = -30$ mV, $I = 0.25$ nA (a); $U = -25$ mV, $I = 0.25$ nA (b); $U = -200$ mV, $I = 0.4$ nA (c); $U = -45$ mV, $I = 0.25$ nA (d). The STM images were background subtracted and smoothed by 5×5 matrix.

conditions [24,26,27], only one of two carbon atoms is resolved in HOPG(0001) STM images (fig. 3(a)). Partial density of electron states (PDOS) calculations, performed for a 20-layer graphite slab within the tight-binding (TB) method (fig. 4)[1], show that both α and β atoms have p_z electron states near the Fermi level (E_F) that are suitable for studies of the fine tip electronic structure effects in SPM. The subatomic features with two-, three-, and

[1]The TB parameters for s- and p-states of graphite were taken from the tables given in the book of Harrison [28] with the $V_{pp\sigma}$ coefficient reduced by a factor of 2 as suggested in Problem 3.3 in Chapt. 3 of that book. The interactions within three nearest-neighbor coordination spheres were taken into account.

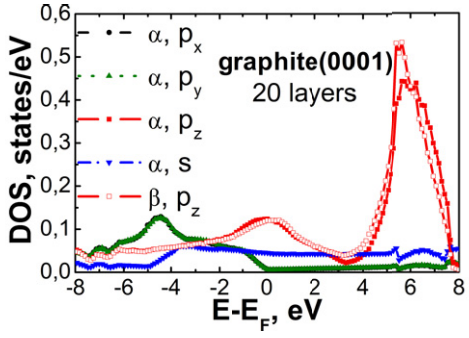

Fig. 4: (Color online) Partial DOS associated with s- and p-orbitals of graphite(0001) surface atoms.

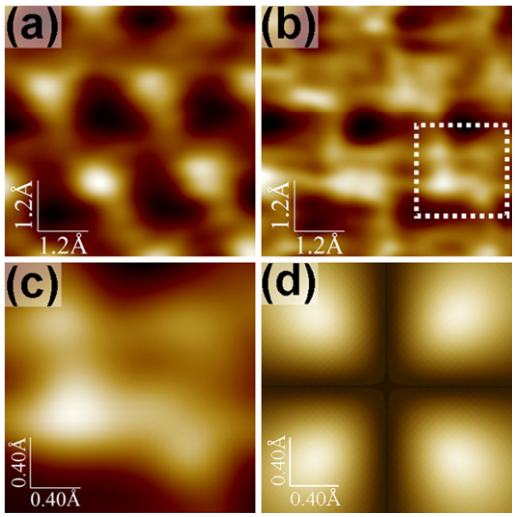

Fig. 5: (Color online) (a), (b) $6\times6\,\text{Å}^2$ STM images of HOPG(0001) surface measured with W[001] tip at $I=0.7\,\text{nA}$ (a) and $I=1.6\,\text{nA}$ (b). $U=-100\,\text{mV}$. (c) A $2\times2\,\text{Å}^2$ region indicated by the dashed square in panel (b). (d) Electron probability density distribution for the W $5d_{x^2-y^2}$-orbital in the plane $z=1.0\,\text{Å}$ from the nucleus. This plane was selected because of necessity of extremely small tip-sample separations for subatomic imaging and due to the fact that carbon orbitals are less localized than tungsten orbitals (see text and fig. 8).

four-fold symmetry have been observed previously in AFM experiments [16] and explained by [011]-, [111]-, and [001]-oriented clusters at the apex of polycrystalline W tips. Similar subatomic features were observed in our STM experiments with polycrystalline W tips (fig. 3(b)–(d)).

In order to improve resolution, we used W[001] tips, which would be more stable because of higher apex atom coordination and would reveal a greater number of details on the subatomic scale [16]. In experiments with W[001] tips (fig. 5(b)) we reproducibly acquired STM images demonstrating a regular lattice of well-resolved four-fold split subatomic features although for most tunneling conditions typical hexagonal patterns (fig. 5(a)) were observed. The experimental image in fig. 5(c) qualitatively reproduces the shape of the W $5d_{x^2-y^2}$ electron orbital calculated within the Thomas-Fermi approximation shown

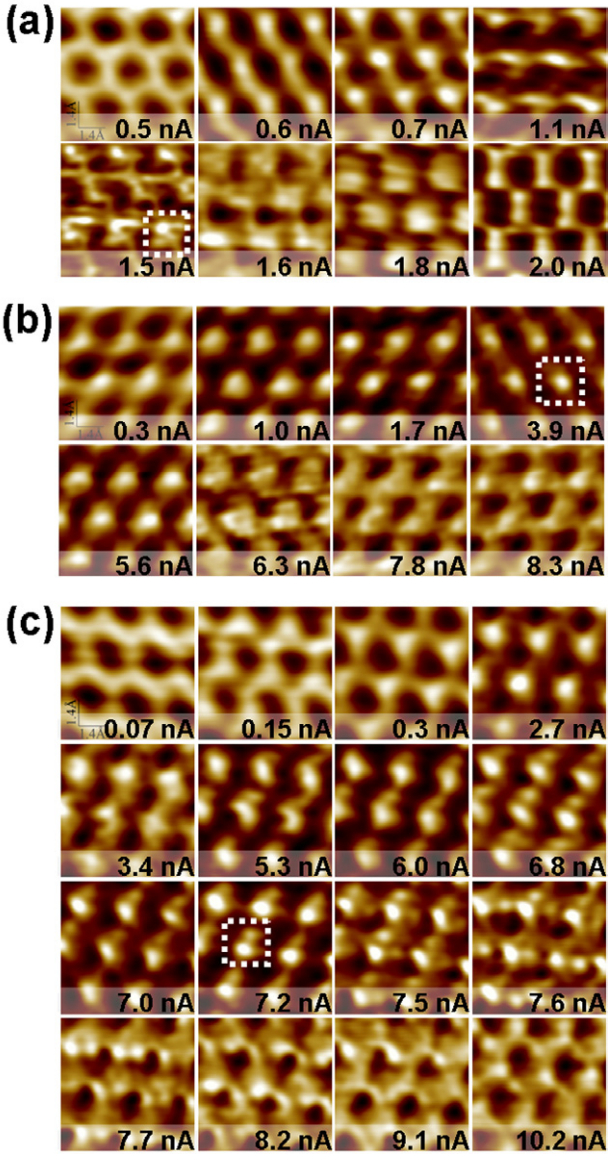

Fig. 6: (Color online) (a)–(c) Gap resistance (tip-sample separation) dependence of $7\times7\,\text{Å}^2$ HOPG(0001) STM images measured with W[001] tips at three bias voltages of $-100\,\text{mV}$ (a), $+23\,\text{mV}$ (b), and $-35\,\text{mV}$ (c). The tunnelling currents are indicated on each particular frame. The images were background subtracted and smoothed by 5×5 matrix. The dashed squares in panels (a), (b) and (c) indicate the regions shown in fig. 2(d), 2(b), and 2(c), respectively.

in fig. 5(d). The difference between the calculated and experimental features (fig. 5(b), (d)) could be caused by a slight tip tilting and strong tip-sample interaction affecting the tip electronic structure and increasing experimental noise because of graphite surface layer oscillations [29].

The observation of four subatomic maxima was found to be both bias and gap resistance dependent. The bias voltage allows to select the range of energies of the electron states involved in the tunneling. The partial density of electron states for the W[001] tip (fig. 13 of ref. [22]) suggests that one can apply a bias voltage

in the way that either the $d_{x^2-y^2}$ or $d_{3z^2-r^2}$ states of the tip could provide maximum contributions. Small positive voltages (up to 50 mV) would be optimal for achieving highest lateral resolution because of large PDOS associated with $d_{3z^2-r^2}$ tip states slightly below E_F [22]. In contrast, at a sample bias around −100 mV one can expect a significant contribution from the $d_{x^2-y^2}$-orbital (fig. 5(b), (c)). The ideal situations when $d_{3z^2-r^2}$ or $d_{x^2-y^2}$ atomic orbitals of the tip can be responsible for STM imaging are shown in fig. 7(b). In fact, we could resolve STM images with four-fold split atomic features at small negative voltages (up to −150 mV). Additionally, the spatial distribution of electron wave functions can result in a strong dependence of STM images on the tip-sample distance [21,30,31]. This is illustrated by gap resistance dependences of HOPG(0001) STM images at different bias voltages shown in fig. 6. The biases were selected on the basis of PDOS calculations [22], to achieve situation when tunneling current is controlled by $d_{x^2-y^2}$ (fig. 6(a)), $d_{3z^2-r^2}$ (fig. 6(b)) or a sum of different d-states (fig. 6(c)).

For all sequences at larger distances (smaller currents) the honeycomb pattern is resolved in accordance with TB calculations (fig. 4). With increasing current (*i.e.* decreasing distance) it transforms into a hexagonal pattern where every second carbon atom is resolved [24]. However, the most interesting results were obtained at smaller gap resistances.

For $U = -100$ mV, at intermediate gap resistances (fig. 6(a), $I = 0.7$ nA) the $d_{3z^2-r^2}$-orbital of the tip is mainly responsible for the observed images with spherically symmetric atomic features. Then, with increasing current the atomic features become asymmetric and at some currents (fig. 6(a), $I = 1.6$ and 1.7 nA) four-fold split subatomic features are observed due to the substantial contribution of $d_{x^2-y^2}$-orbital. The images in fig. 2(d) and 5(c) correspond to the situation when this tip orbital is responsible for the STM imaging. Evidently, this can be achieved by a suitable choice of both voltage and distance (fig. 6).

The best resolution can be achieved when the tip $d_{3z^2-r^2}$-orbital is responsible for the tunnelling current. This is demonstrated by the measurements at a sample bias of +23 mV (fig. 6(b)). One can see an enhancement of lateral resolution at tunneling currents between 1.0 and 3.9 nA. The most impressive resolution is achieved at $I = 3.9$ nA (fig. 6(b)) when the full width at half maximum of the atomic features is slightly below 1 Å. This is close to the physical limit of the resolution related to the spatial distribution of the carbon p_z-orbital. The left part of fig. 2(a) illustrates the situation when the p_z-orbital is imaged with the $d_{3z^2-r^2}$-orbital. With decreasing distance, the atomic features become broader but distinct subatomic features could not be resolved unambiguously.

The most informative tip-sample distance dependence was obtained at $U = -35$ mV which is partially shown in fig. 6(c). Firstly, one can see an enhancement of the resolution with decreasing distance. Then, the atomic features

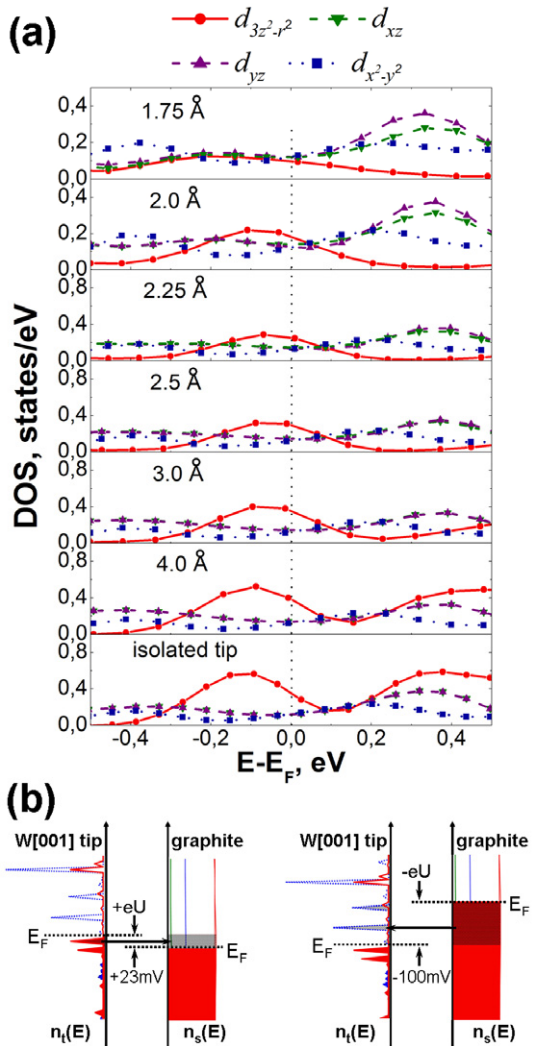

Fig. 7: (Color online) (a) PDOS associated with different d-orbitals of the W[001] tip apex atom interacting with the graphite(0001) surface. The distances between tip and surface atom nuclei are indicated on each panel. (b) Schematic models of the tunnelling process in the W[001] tip-graphite(0001) system for STM imaging in the empty (left panel) and occupied (right panel) surface state regimes. The PDOS for the models (b) was taken from ref. [22].

become smeared and at some currents (≈ 5.3 nA) transformed into double features. Then, in the current range from 5.3 to 7.2 nA the double features become sharper. And finally, they are rapidly transformed into features with four-fold symmetry (7.7–9.1 nA). It is seen that in a very narrow range of the tunneling currents, the subatomic features demonstrate a three-fold symmetry (7.5–7.6 nA) that can be related to simultaneous contribution of both $d_{xz,yz}$ and $d_{x^2-y^2}$ electron orbitals. This sequence proves that explanation based on the tip cluster orientation [16] can only be partially correct and is not valid in general case: Different subatomic features can be resolved with the same tip while the most frequently observed double features can be measured in a significantly wider range

of the tip-sample distances. The STM image transformation shown in fig. 6(c) is determined by two factors: i) the difference in spatial localization of d-orbitals with different m which implies that they can be probed by a carbon p_z-orbital at different tip-sample separations and ii) gradually decreasing density of states (DOS) on the further extended tip orbitals ($d_{3z^2-r^2}$ and then $d_{xz,yz}$) because of their substantial overlapping with the carbon p_z-orbital. At small distances the PDOS associated with the tip $d_{3z^2-r^2}$-orbital becomes smaller and the experimental conditions can correspond to the models depicted in the central and right parts of fig. 2(a). In these cases two or four distinct maxima can be resolved typical for the $d_{xz,yz}$ (fig. 2(c)) and $d_{x^2-y^2}$ (fig. 2(d)) wave functions.

To prove this interpretation we have performed DFT calculations of the PDOS at the W tip atom interacting with the graphite cluster. The *ab initio* DOS calculations were performed using the VASP program. A plane augmented wave basis [32] was used with an energy cutoff of 400 eV. The electron exchange and correlation was simulated by local density approximation pseudopotentials with a Ceperley-Alder exchange functional [33]. A Γ centered $(1 \times 1 \times 1)$ k-point grid was used for all calculations to sample the Brillioun zone. For the DOS a smearing of 0.2 eV was applied using the Methfessel-Paxton method. The global break condition for the electronic self consistent loops was set to a total energy change of less than $1 \cdot 10^{-6}$ eV.

The simulated graphite(0001) surface consisted of two constrained unit layer slabs. To model the W tip we used a pyramid in [001] orientation out of seven unit layer slabs (128 atoms in total). For the tip all atom positions were constrained as well. Tip-sample separations from 1.25 Å up to 4.0 Å were applied to calculate the PDOS dependence on the distance. The spacing between the back of the tip slab and the HOPG was ≈ 7.5 Å for a distance of 4 Å, for all other distances it was correspondingly larger.

The results of DFT calculations presented in fig. 7(a) are in a good agreement with the above discussion. The PDOS associated with the $d_{3z^2-r^2}$-orbital decreases drastically when the separation is close to the interatomic distances (below 3.0 Å). The tip $d_{x^2-y^2}$-orbital can dominate at small distances and small negative bias voltages, while d_{xz} and d_{yz} orbitals are not equivalent at distances below 2.25 Å due to the tip-sample interaction, which can lead to doubling subatomic features. Note that PDOS calculations of the fully relaxed W[001] tip-graphite system (to be published elsewhere) give qualitatively the same results. According to the DFT calculations (fig. 7(a)), the best lateral resolution can be obtained at small positive sample biases and distances around 3 Å, but four-fold splitting can, in principle, be resolved at very small gap spacings in some ranges of the bias voltages. However, at negative biases from -50 to -150 mV the four-fold splitting can be achieved at somewhat greater distances because the DOS

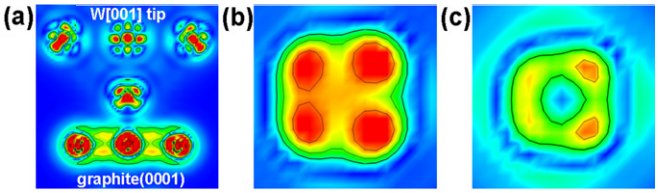

Fig. 8: (Color online) (a)–(c) Calculated electron density distribution for the W[001] tip atom interacting with a graphite(0001) atom shown as a (100) slice through the apex atom (a) and 2×2 Å^2 (001) slices located 0.4 Å (b) and 0.6 Å (c) below the apex atom. The asymmetrical orbitals in panels (b) and (c) are due to the tip interaction with the surface which is not two-fold symmetrical along the tip axis.

associated with the $d_{x^2-y^2}$ tip orbital exceeds the DOS for other orbitals in the corresponding energy interval of the empty tip electron states (fig. 6(a)). We assume that the strong tip-sample interaction, inducing uncontrollable fluctuations of the gap spacing at small distances [29], is the most probable reason why the four-fold splitting could not be observed clearly at positive bias voltages in our experiments. In contrast, the splitting was evident at negative biases (*e.g.*, see fig. 5 and fig. 6(a), (c)) although the appearance of the four-fold split features is not fully identical. The latter is tightly related to the fact that appearance of four distinct subatomic maxima is essentially distance dependent: very small change in the tip-sample separation can easily modify the shape of the subatomic features or even completely suppress the effect. We illustrate this by calculated electron density maps for the fully-relaxed W[001] tip-graphite system shown in fig. 8. In this case the final W-C interatomic distance is 2.38 Å (1.75 Å before allowing atomic relaxations). This slightly exceeds the W-C bond length in tungsten carbide and can be realized in experiments. Figure 8(a) reveals that carbon orbitals protrude much further into vacuum than tungsten d-orbitals. For that reason even the highly localized W $d_{x^2-y^2}$-orbital (fig. 8(b)) can be probed by carbon orbitals. Comparison of the calculated electron density maps in (001) planes located 0.4 and 0.6 Å below the apex core (fig. 8(b), (c)) shows that transition from imaging two-fold to imaging four-fold split subatomic features requires a small (around 0.2 Å) change in the tip-sample separation. This is in line with the tunneling current values indicated in fig. 6(c). The experimental tip-sample distances corresponding to imaging particular electron orbitals of the W[001] tip atom can be estimated from the distance dependence of STM images (fig. 6) and PDOS calculations shown in fig. 7(a). It is reasonable to assume that spherically symmetric features start to smear out at gap spacings corresponding to fading PDOS associated with the $d_{3z^2-r^2}$-orbital. This is observed at distances slightly below 3.0 Å. For our experiments these distances correspond to tunneling currents of 0.7 nA, 3.9 nA and 2.7 nA at bias voltages of -100 mV, $+23$ mV

and −35 mV, respectively. From the values of tunneling currents required for imaging symmetric and four-fold split features (fig. 6(a), (c)), and assuming the exponential distance dependence, one can suggest that four-fold and two-fold split subatomic features are observed in the tip-surface separation range of 2.0–2.5 Å. The observed rapid transition from symmetric to multiple subatomic features can be one of the reasons why subatomic contrast was earlier detected with AFM but could not be observed in simultaneous STM experiments [16]: the required distance was not reached in the STM regime but occurred during the tip-surface approaching phase of the probe vibrations in the AFM mode.

For all dependences, at the smallest distances one can see a reverse transformation from hexagonal to honeycomb pattern (lower panels in fig. 6(a)–(c)). This is consistent with a "current-distance" dependence observed in [27]. In this regime the honeycomb patterns can mostly be determined by the repulsive tip-sample interaction due to drastically decreased PDOS near E_F (fig. 7).

In conclusion, one can fabricate a single crystalline tip with a certain set of wave functions at the apex and adjust the tunneling parameters to select one of them for STM imaging. Note that a tip suitable for high-resolution studies on one surface may not be as effective on another sample because of the necessity of applying different bias voltages. The relative contributions of different atomic orbitals are simultaneously bias- and distance-dependent because of the overlapping of the tip and sample wave functions. STM topographic images can bear important information on the tip and surface electronic structure that cannot be obtained even with sophisticated spectroscopic techniques. And finally, the single-electron wave functions can be probed in real space and controllably selected for high-resolution STM studies. This possibility can provide key to success in improving spatial resolution and controllable chemical analysis on an atomic scale.

* * *

This work was supported by RAS and RFBR grants and SFI E. T. S. Walton Programme. One of the authors (ANC) thanks W. A. Hofer for helpful discussion.

REFERENCES

[1] Binnig G., Rohrer H., Gerber Ch. and Weibel E., *Appl. Phys. Lett.*, **40** (1982) 178.
[2] Binnig G. and Rohrer H., *Helv. Phys. Acta*, **55** (1982) 726.
[3] Binnig G., Quate C. F. and Gerber Ch., *Phys. Rev. Lett.*, **56** (1986) 930.
[4] Binnig G., Rohrer H., Gerber Ch. and Weibel E., *Phys. Rev. Lett.*, **49** (1982) 57.
[5] Eigler D. M. and Schweizer E. K., *Nature*, **344** (1990) 524.
[6] Schmid M., Stadler H. and Varga P., *Phys. Rev. Lett.*, **70** (1993) 1441.
[7] Chaika A. N. and Bozhko S. I., *JETP Lett.*, **72** (2005) 416.
[8] Wiesendanger R., Güntherodt H.-J., Güntherodt G., Gambino R. J. and Ruf R., *Phys. Rev. Lett.*, **65** (1990) 247.
[9] Fowler R. H. and Nordheim L. W., *Proc. R. Soc. A*, **119** (1928) 173.
[10] Tersoff J. and Hamann D. R., *Phys. Rev. Lett.*, **50** (1983) 1998.
[11] Tersoff J. and Hamann D. R., *Phys. Rev. B*, **31** (1985) 805.
[12] Chen C. J., *Phys. Rev. Lett.*, **65** (1990) 448.
[13] Chen C. J., *Phys. Rev. B*, **42** (1990) 8841.
[14] Chen C. J., *Phys. Rev. Lett.*, **69** (1992) 1656.
[15] Giessibl F. J., Hembacher S., Bielefeldt H. and Mannhart J., *Science*, **289** (2000) 422.
[16] Hembacher S., Giessibl F. J. and Mannhart J., *Science*, **305** (2004) 380.
[17] Herz M., Giessibl F. J. and Mannhart J., *Phys. Rev. B*, **68** (2003) 045301.
[18] Zotti L. A., Hofer W. A. and Giessibl F. J., *Chem. Phys. Lett.*, **420** (2006) 177.
[19] Chaika A. N. and Myagkov A. N., *Chem. Phys. Lett.*, **453** (2008) 217.
[20] Chaika A. N., Semenov V. N., Nazin S. S., Bozhko S. I., Murphy S., Radican K. and Shvets I. V., *Phys. Rev. Lett.*, **98** (2007) 206101.
[21] Murphy S., Radican K., Shvets I. V., Chaika A. N., Semenov V. N., Nazin S. S. and Bozhko S. I., *Phys. Rev. B*, **76** (2007) 245423.
[22] Chaika A. N., Nazin S. S. and Bozhko S. I., *Surf. Sci.*, **602** (2008) 2078.
[23] Chaika A. N., Semenov V. N., Glebovskiy V. G. and Bozhko S. I., *Appl. Phys. Lett.*, **95** (2009) 173107.
[24] Whangbo M.-H., Liang W., Ren J., Magonov S. N. and Wawkuschewski A., *J. Chem. Phys.*, **98** (1994) 7602.
[25] Horcas I., Fernandez R., Gomez-Rodriguez J. M., Colchero J., Gomez-Herrero J. and Baro A. M., *Rev. Sci. Instrum.*, **78** (2007) 013705.
[26] Atamny F., Spillecke O. and Schlogl R., *Phys. Chem. Chem. Phys.*, **1** (1999) 4113.
[27] Hembacher S., Giessibl F. J., Mannhart J. and Quate C. F., *Phys. Rev. Lett.*, **94** (2005) 056101.
[28] Harrison W., *Electronic Structure and the Properties of Solids* (W. H. Freeman and Co., San Francisco) 1980.
[29] Binnig G. K., *Phys. Scr.*, **T19** (1987) 53.
[30] Bode M., Pascal R. and Wiesendanger R., *Z. Phys. B*, **101** (1996) 103.
[31] Calleja F., Arnau A., Hinarejos J. J., Vazquez de Parga A. L., Hofer W. A., Echenique P. M. and Miranda R., *Phys. Rev. Lett.*, **92** (2004) 206101.
[32] Kresse G. and Furthmüller J., *Phys. Rev. B*, **54** (1996) 11169.
[33] Ceperley D. M. and Alder B. J., *Phys. Rev. Lett.*, **45** (1980) 566.